

DroneKey: Drone 3D Pose Estimation in Image Sequences using Gated Key-representation and Pose-adaptive Learning

Seo-Bin Hwang¹ and Yeong-Jun Cho^{1*}

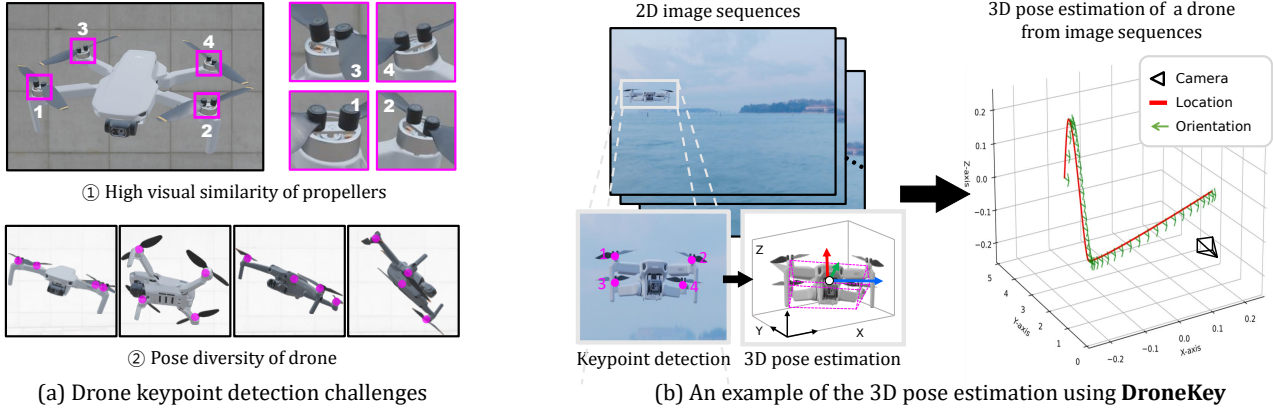


Fig. 1: Overview of drone keypoint detection and 3D pose estimation. (a) Challenges in drone keypoint detection. (b) Pipeline and result of 3D pose estimation from 2D image sequences through keypoint detection and 3D pose estimation.

Abstract—Estimating the 3D pose of a drone is important for anti-drone systems, but existing methods struggle with the unique challenges of drone keypoint detection. Drone propellers serve as keypoints but are difficult to detect due to their high visual similarity and diversity of poses. To address these challenges, we propose DroneKey, a framework that combines a 2D keypoint detector and a 3D pose estimator specifically designed for drones. In the keypoint detection stage, we extract two key-representations (intermediate and compact) from each transformer encoder layer and optimally combine them using a gated sum. We also introduce a pose-adaptive Mahalanobis distance in the loss function to ensure stable keypoint predictions across extreme poses. We built new datasets of drone 2D keypoints and 3D pose to train and evaluate our method, which have been publicly released. Experiments show that our method achieves an AP of 99.68% (OKS) in keypoint detection, outperforming existing methods. Ablation studies confirm that the pose-adaptive Mahalanobis loss function improves keypoint prediction stability and accuracy. Additionally, improvements in the encoder design enable real-time processing at 44 FPS. For 3D pose estimation, our method achieved an MAE-angle of 10.62°, an RMSE of 0.221m, and an MAE-absolute of 0.076m, demonstrating high accuracy and reliability. The code and dataset are available at <https://github.com/kkanuseobin/DroneKey>.

I. INTRODUCTION

In recent years, drones have been widely used across various domains, including videography, delivery, and military applications. However, their misuse for illegal purposes has also been increasing. To address this issue, an anti-drone system [1] has been proposed, which estimates a drone’s 3D pose (i.e., position and orientation). Estimating a drone’s 3D pose also allows for determining its gaze

direction and position, which are crucial for assessing its potential illegality.

Various studies have explored estimating a drone’s 3D pose from single-camera images. For example, G. Albanis et al. [2] proposed a 3D pose estimation method based on silhouette analysis. However, due to the symmetrical drone appearance, this method cannot accurately estimate drone orientations. To address this issue, previous studies [3], [4] have explored detecting 2D keypoints as a more reliable approach for 3D pose estimation. This approach is effective because keypoints represent the drone’s 3D pose and allow for 3D pose reconstruction using geometric computations (e.g., PnP solver [21]) as depicted in Fig. 1 (b).

However, detecting 2D keypoints from drone images presents two challenges. First, drone keypoints, particularly propellers, exhibit high visual similarity, as shown in Fig. 1 (a)-①. The high visual similarity of propellers makes it difficult to determine their order and arrangement. In keypoint detection, it is crucial not only to locate keypoints but also to infer their correct order. Second, drones have diverse poses, as shown in Fig. 1 (a)-②. Unlike humans or vehicles, drones can freely rotate in the air. In the case of humans, keypoint positions are predictable; for example, the head is above the shoulders, and both legs are positioned lower. However, for drones, keypoints are arranged more freely, making it difficult to predict their position and order.

In this study, we employ a transformer [5] structure as the baseline for the proposed DroneKey to leverage its ability to capture both spatial relationships and keypoint orders. Since transformers tend to focus on object-level features [6], we need to extract compact representations of keypoint shapes to enhance spatial locality. Moreover, to efficiently train the

¹Department of AI Convergence, Chonnam National University, Korea. cnu.cv1.hsb@gmail.com and yj.cho@jnu.ac.kr

*Corresponding Author

large number of network parameters in the transformer with a limited amount of training data, we maximized the use of mid-level features from the transformer encoder. To this end, we propose a novel keypoint head with the following approach: by utilizing all encoder layers, we incorporate diverse features to enhance keypoint detection. We employ gated sum integration to learn the importance of each layer, allowing for optimal weight assignment and more effective training. As a result, keypoints for all propellers with similar visuals can be accurately detected in the correct order.

Furthermore, to improve keypoint detection in extreme drone poses, we propose a pose-adaptive Mahalanobis distance for our loss function. To this end, we analyze the arrangement of drone keypoints by computing the covariance matrix, which represents their alignment according to pose variations. Based on the covariance matrix, we compute the Mahalanobis distance in our loss function to adaptively assess each keypoint error relative to the drone's pose. To enhance the stability of the loss function, we design the loss function to be adjustable using the proposed scale function over the training time.

To validate the proposed methods, we provide new drone datasets, such as 2DroneKey and 3DronePose, and extensively evaluate them by comparing them with other state-of-the-art methods. Our proposed DroneKey offers a pipeline from 2D keypoint detection to 3D pose estimation in image sequences, as shown in Fig. 1 (b). The main contributions of this study are as follows:

- **First study on drone-specific keypoint detection:** Unlike prior works using general methods, we propose a framework tailored to drone keypoint detection.
- **Provide a new dataset:** We created and released a synthetic dataset using real-world 360-degree footage as backgrounds to address the lack of drone keypoint and 3D pose datasets.
- **Real-time performance:** With an optimized architecture and 6 encoder layers, our model achieves 44 FPS.
- **High accuracy:** Our method achieved an AP of 99.68% (OKS) [7]. The estimated 3D pose showed minimal errors, achieving an MAE-angle of 10.62°, an RMSE of 0.221m, and an MAE-absolute of 0.076m.

These results enable 3D drone pose estimation from 2D images, making the proposed method suitable for anti-drone applications requiring 3D pose information.

II. RELATED WORKS

The objectives of this study are 2D keypoint detection in image sequences and 3D pose estimation of the drone. Drone 3D pose estimation methods using 2D images and keypoint detection methods are reviewed in this section.

A. Drone 3D Pose Estimation using 2D Images

Estimating a drone's 3D pose (i.e., 3D position and orientation) using only a single camera is challenging. From a geometric perspective, at least two cameras or depth-based sensors are required to determine 3D pose. Nevertheless,

estimating 3D pose using only a single RGB camera is highly practical, making it a widely studied topic in recent research. Fu et al. [8] proposed a drone pose estimation based on tracking markers attached to the drone. However, this method requires known markers on the drone, which limits its practicality. Albanis et al. [2] estimated the 3D pose of a drone using its silhouette mask without requiring markers. However, this method easily confuses the drone's orientation due to the drone's symmetric appearance. These methods lack practicality and accuracy.

To address these issues, many studies have focused on extracting keypoints from 2D images and estimating 3D pose based on the extracted keypoints. For drones, the primary keypoints are the propellers. Since their arrangement directly reflects the drone's orientation and position. To this end, Jin et al. [3] proposed drone keypoint detection by using mask R-CNN [16]. You et al. [4] proposed a simple coordinate classification (SimCC) [13] for drone keypoint detection. These studies [3], [4] merely applied existing object detection methods for drone keypoint detection. However, they did not fully account for the challenges of drone keypoint extraction as shown in Fig. 1 (a).

B. Keypoint Detection

Keypoint detection has been studied for 2D pose estimation of objects. Since keypoints are represented in coordinate space, they are typically predicted using coordinate regression. Toshev et al. [9] proposed a keypoint detection using deep neural network regression of keypoint coordinates. However, this keypoint regression approach is challenging because it requires predicting the exact position of a keypoint within an $H \times W$ image. This means the model must determine a precise coordinate for all possible keypoint positions. Its limitation is failing to model probabilistic distributions, making it sensitive to pixel shifts and ambiguous keypoints.

To address this issue, Tompson et al. [14] proposed a heatmap regression model. By regressing on a ground truth heatmap, this approach handles keypoint uncertainty and improves learning in high-dimensional space. In another study, Xu et al. [10] enhanced keypoint detection by using vision transformer (ViT) [11] as a backbone. Similarly, Li et al. [12] propose a method that generates tokens containing keypoint heatmaps. However, heatmap regression struggles to accurately generate the ground-truth heatmap at low-resolution images. While higher resolutions improve accuracy, they also increase computational cost.

We reviewed studies on drone 3D pose estimation and keypoint detection. Existing methods did not fully consider keypoint detection challenges (Fig. 1 (a)). Keypoint detection methods lack consistency due to pixel sensitivity and resolution dependence. To address these issues, we used a transformer network to learn relationships between keypoints. In addition, we designed a novel pose-adaptive Mahalanobis loss to address challenges in drone keypoint detection and enhance training efficiency. This proposed loss integrates the benefits of both coordinate regression and heatmap regression.

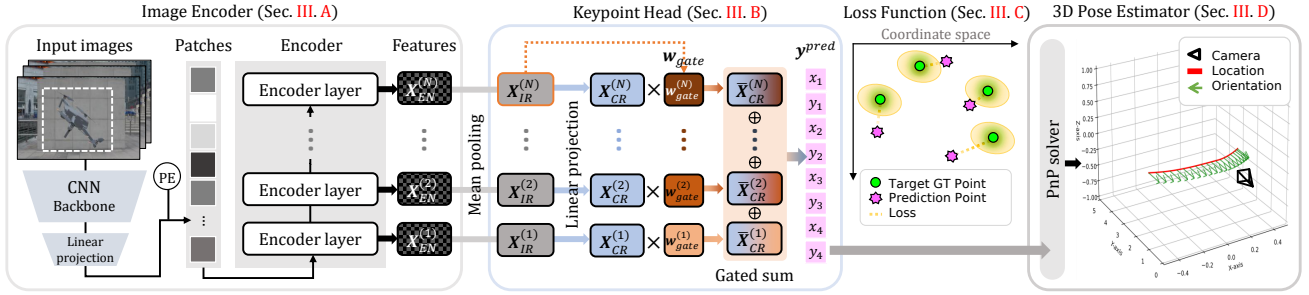


Fig. 2: Overall framework for drone keypoint detection and 3D pose estimation.

III. PROPOSED METHODS

The proposed 3D drone pose estimation framework, named DroneKey, consists of four components, as shown in Fig. 2. It detects the four propellers of the drone as keypoints for estimating the drone’s 3D pose. Then, the drone’s 3D pose is geometrically computed using a PnP solver.

A. Image Encoder for Extracting Representative Features

CNN-based methods [16]–[18] mainly focus on learning local visual features, limiting their ability to capture relationships between keypoints. However, as described in Sec. I, the drone’s keypoints (i.e., propellers) have the same appearance. While CNN-based methods can detect individual propellers, they cannot predict their spatial arrangement for pose estimation. To handle this issue, we employ a transformer encoder [5] with self-attention to learn global keypoint relationships. A CNN backbone extracts a feature \mathbf{X} from the input image $\mathbf{I} \in \mathbb{R}^{H \times W \times C}$, where H and W denote the height and width of the image, respectively, and C represents the number of channels. The extracted feature from the CNN backbone can be represented as $\mathbf{X} \in \mathbb{R}^{\frac{H}{32} \times \frac{W}{32} \times d}$, where d denotes the feature dimension. The feature is simply tokenized as $\mathbf{x}_p \in \mathbb{R}^d$, where $p = 1, 2, \dots, P$, denotes the index of the visual token, and $P = \frac{H}{32} \times \frac{W}{32}$.

Before inputting the visual token \mathbf{x}_p into the transformer encoder, positional encoding (PE) is added to preserve spatial information by $\mathbf{x}_p^{(0)} = \text{PE}(\mathbf{x}_p) + \mathbf{x}_p$. A set of input visual tokens $\mathbf{X}^{(0)} = \{\mathbf{x}_1^{(0)}, \mathbf{x}_2^{(0)}, \dots, \mathbf{x}_P^{(0)}\}$ is then processed through the self-attention transformer layers as follows:

$$\mathbf{X}^{(l)} = \text{selfAttention}(Q = \mathbf{X}^{(l-1)}, K = \mathbf{X}^{(l-1)}, V = \mathbf{X}^{(l-1)}), \quad (1)$$

where Q , K , V are query, key, and value for self-attention inputs, respectively, and $l = 1, 2, \dots, N$ represents the index of the self-attention layer. We follow the transformer encoder structure as proposed in [5]. It stacks N self-attention layers with fully connected layers (FCN) to construct the transformer encoder, enabling it to capture visual relationships between input visual tokens. Thus, the output of each encoder can be represented by $\mathbf{X}_{EN}^{(l)} = \text{FCN}(\mathbf{X}^{(l)})$.

B. Keypoint Head for Detecting 2D Keypoint Positions

The final output of the image encoder, $\mathbf{X}_{EN}^{(N)}$, contains high-level contextual information learned through multiple self-attention layers. In general, only the output from the final layer $\mathbf{X}_{EN}^{(N)}$ is used. However, inspired by previous works [19],

[20] that leveraged mid-level feature representations, we utilize all feature representations, i.e., $\{\mathbf{X}_{EN}^{(1)}, \mathbf{X}_{EN}^{(2)}, \dots, \mathbf{X}_{EN}^{(N)}\}$.

To utilize all the mid-level feature representations in the keypoint heads, we further transform them as follows. First, we apply mean pooling to each feature representation along the feature dimension.

$$\mathbf{X}_{IR}^{(l)} = \frac{1}{P} \sum_{p=1}^P \mathbf{x}_p^{(l)}, \quad (2)$$

where $\mathbf{x}_p^{(l)}$ is the p -th visual token of l -th encoder layer output $\mathbf{X}_{EN}^{(l)}$. We call this averaged feature representation intermediate representation (IR). Then, $\mathbf{X}_{IR}^{(l)} \in \mathbb{R}^d$ aggregates information from multiple patches into a unified representation, summarizing the features learned at each layer.

Second, we further apply linear projection to $\mathbf{IR}^{(l)}$ as follows:

$$\mathbf{X}_{CR}^{(l)} = \mathbf{W} \cdot \mathbf{X}_{IR}^{(l)} + \mathbf{b}, \quad (3)$$

where $\mathbf{W} \in \mathbb{R}^{2K \times d}$ is a trainable weight matrix and \mathbf{b} is a bias vector. Here, K represents the number of keypoints in drones and $2K$ corresponds to the two-dimensional coordinates (x, y) of these keypoints. We set $K = 4$ since the keypoints correspond to the drone propellers. We call the $2K$ -dimensional features the compact representation (CR), which is aligned with the dimension of the ground truth coordinate values.

To effectively aggregate the $\mathbf{X}_{CR}^{(l)}$ extracted from each encoder layer, we employ a gated summation method. To this end, we generate a weight vector from the intermediate representation of the final layer, $\mathbf{X}_{IR}^{(N)}$, by applying a linear projection and softmax function, as follows:

$$\mathbf{w}_{\text{gate}} = \text{softmax}(\mathbf{W}^g \cdot \mathbf{X}_{IR}^{(N)} + \mathbf{b}^g), \quad (4)$$

where $\mathbf{W}^g \in \mathbb{R}^{N \times d}$ is a trainable weight matrix and \mathbf{b}^g is a bias vector. Then, the N -dimensional weight vector \mathbf{w}_{gate} is element-wise multiplied with each layer’s $\mathbf{X}_{CR}^{(l)}$ as follows:

$$\bar{\mathbf{X}}_{CR}^{(l)} = \mathbf{w}_{\text{gate}}^{(l)} \mathbf{X}_{CR}^{(l)}, \quad (5)$$

where $\mathbf{w}_{\text{gate}}^{(l)}$ denotes l -th weight value in the \mathbf{w}_{gate} . We then aggregate the weighted compact representations by $\mathbf{X}_G = \sum_{l=1}^N \bar{\mathbf{X}}_{CR}^{(l)}$. This aggregated representation effectively integrates crucial information extracted from all layers, resulting in a richer and more informative representation. Finally, the gated summation result, $\mathbf{X}_G \in \mathbb{R}^{2K}$, is passed through the

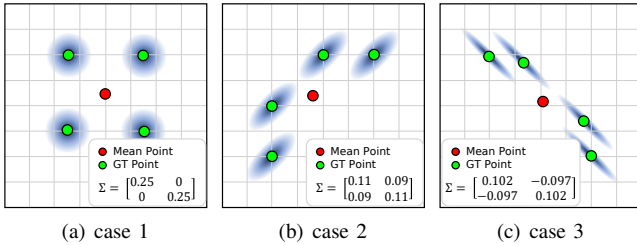


Fig. 3: **Distributions of keypoints and their covariance matrices.**

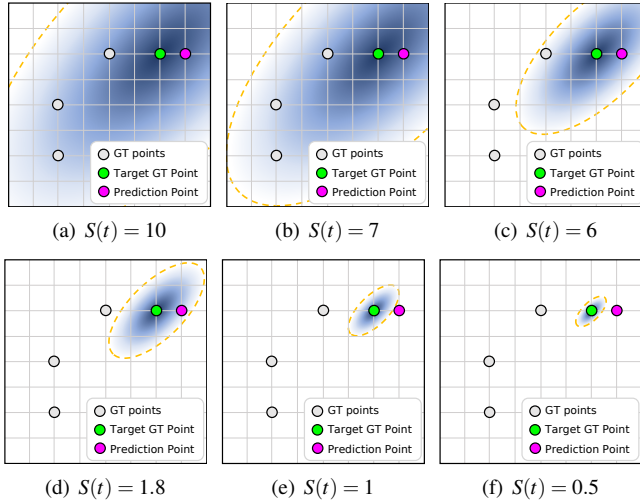


Fig. 4: **Effect of scale values in pose-adaptive Mahalanobis distance.** As the scale value increases, the allowable range expands, whereas a narrower distribution leads to convergence toward a stricter loss.

rectified linear unit (ReLU) function to predict the final keypoint coordinates as the following equation.

$$\mathbf{y}^{pred} = \text{ReLU}(\mathbf{X}_G), \quad (6)$$

where the ReLU function sets negative values to zero, enabling the model to learn stable key-representations and preventing unrealistic negative coordinate predictions.

C. Pose-adaptive Mahalanobis Loss

To optimize the networks, including the encoder (Sec. III.A) and keypoint heads (Sec. III.B), for accurate keypoint detection in drones, we considered two issues when designing the loss function. First, the drone exhibited pose diversity, requiring keypoint prediction to be adaptive to variations in pose. Second, the proposed loss must converge stably and achieve a good solution. Thus, our loss function accounted for both aspects: adaptability and stability for the drone keypoint detection problem.

For adaptability, we design a loss function that dynamically adjusts to keypoint position changes according to variations in the drone's pose. To achieve this, we analyze the arrangement of the ground-truth drone keypoints by computing the covariance matrix by

$$\Sigma = \frac{1}{K} \sum_{k=1}^K (\mathbf{y}_k^{gt} - \mu)(\mathbf{y}_k^{gt} - \mu)^T \quad (7)$$

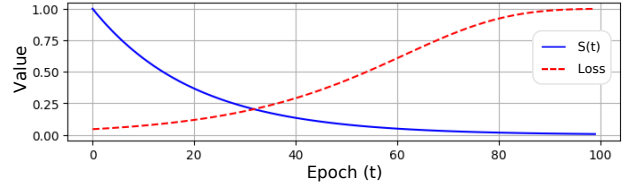


Fig. 5: **Scale value and loss over epochs (t).** The plot illustrates the evolution of scale value (—) and loss (---) over training epochs.

where K is the number of keypoints and μ is the average coordinates. This covariance matrix represents the distribution of drone keypoints as shown in Fig. 3. Therefore, we then measure the Mahalanobis distance between the ground-truth keypoints \mathbf{y}_k^{gt} and predicted keypoints \mathbf{y}_k^{pred} as follows:

$$d(\mathbf{y}_k^{gt}, \mathbf{y}_k^{pred}) = \sqrt{(\mathbf{y}_k^{gt} - \mathbf{y}_k^{pred})^T \Sigma^{-1} (\mathbf{y}_k^{gt} - \mathbf{y}_k^{pred})}. \quad (8)$$

Based on this distance metric, we can adaptively measure each keypoint error relative to the drone's pose.

To enhance the stability of the loss function, we design it to operate differently during the early and late stages of training. Specifically, in the early stages, when the network is not yet well optimized, the loss function is formulated to be more flexible, allowing for smoother convergence. Conversely, in the later stages, the loss function becomes more stringent to enforce precise optimization and improve the model's final performance. To achieve this, we multiply the scale value to the covariance matrix by

$$\Sigma_t = S(t) \Sigma + \epsilon \mathbf{I}, \quad \text{where } S(t) = D e^{-0.01\alpha t}, \quad (9)$$

where α represents the decay factor, and D denotes the scale factor, and t denotes the training epoch. The scale function $S(t)$ exponentially decreases over t . To prevent Σ_t from becoming a zero matrix, a small identity matrix ($\epsilon \mathbf{I}$) was added. Based on this, the covariance matrix Σ_t decreases from a large value to a smaller value over the training epoch t as shown in Fig. 4.

Finally, we reformulate the equation (8) with Σ_t , and the distance function of t is defined as follows:

$$d_t(\mathbf{y}_k^{gt}, \mathbf{y}_k^{pred}) = \sqrt{(\mathbf{y}_k^{gt} - \mathbf{y}_k^{pred})^T \Sigma_t^{-1} (\mathbf{y}_k^{gt} - \mathbf{y}_k^{pred})}. \quad (10)$$

The final loss function based on Gaussian distribution is defined as

$$\mathcal{L}_{\text{pose}}(t) = \mathbb{E} \left[1 - \frac{1}{2\pi|\Sigma_t|^{1/2}} \exp \left(-\frac{1}{2} d_t(\mathbf{y}_k^{gt}, \mathbf{y}_k^{pred}) \right) \right]. \quad (11)$$

The proposed loss function adjusts its computation intensity based on the training epoch t , as shown in Fig. 5. Moreover, the proposed distance $d_t(\mathbf{y}_k^{gt}, \mathbf{y}_k^{pred})$ enables adaptive loss computation based on the drone's pose. Thus, we designed a loss function that considers both adaptability and stability during training. All parameters in our networks are trainable.

D. 3D Pose Estimator

The 3D pose of a drone is represented in 6 degrees of freedom (6DoF). The 6DoF of a drone consists of translation (t_x, t_y, t_z) and rotation angles (r_x, r_y, r_z). The rotation can be

represented by a 3×3 rotation matrix $\mathbf{R}_{pose} \in \mathbb{R}^{3 \times 3}$, and the translation can be represented by a translation vector $\mathbf{t}_{pose} \in \mathbb{R}^{3 \times 1}$. To estimate the 6DoF using the predicted 2D drone keypoints, the keypoint coordinates are transformed into 3D spatial coordinates, as shown in Fig. 6. The image coordinate system contains predicted drone keypoints $\mathbf{y}^{pred} = \{\mathbf{y}_k^{pred}\}_{k=1}^K$, representing detected 2D propeller positions, while the world coordinate system contains corresponding 3D keypoints $\mathbf{Y}^{obj} = \{\mathbf{Y}_k^{obj}\}_{k=1}^K$. Note that, since the type of drone is assumed to be known, the 3D keypoint locations \mathbf{Y}^{obj} of the drone are known. For example, an object detector can be utilized to identify the drone class, and by referring to the specifications of the corresponding drone, the actual 3D positions of the keypoints can be obtained. In addition, the camera is already calibrated, so camera parameters, such as the intrinsic parameters \mathbf{A} , are given.

The transformation from world to camera coordinates is defined by $\mathbf{P}_c = \mathbf{R}\mathbf{X}_w + \mathbf{t}$, where $\mathbf{P}_c = (X_c, Y_c, Z_c)^T$ are camera coordinates. The camera pose (\mathbf{R}, \mathbf{t}) is estimated using the PnP solver [21] by minimizing the re-projection error,

$$\arg \min_{\mathbf{R}, \mathbf{t}} \sum_{k=1}^K \left| \mathbf{y}_k^{pred} - \mathbf{A}(\mathbf{R}\mathbf{Y}_k^{obj} + \mathbf{t}) \right|^2, \quad (12)$$

where \mathbf{A} represents the camera intrinsic matrix. The 3D keypoint position in camera coordinate is reconstructed by

$$\mathbf{Y}_k = \mathbf{R}^{-1}(\mathbf{Y}_k^{obj} - \mathbf{t}). \quad (13)$$

For rotation estimation, the centroid of the four keypoints is computed as $\mathbf{Y}_O = \frac{1}{K} \sum_{k=1}^K \mathbf{Y}_k$. Using this centroid, two-directional vectors are defined: \mathbf{v}_1 is represented by the green line, and \mathbf{v}_2 is represented by the blue line as in Fig. 6.

$$\mathbf{v}_1 = \mathbf{Y}_2 - \mathbf{Y}_O, \quad \mathbf{v}_2 = \mathbf{Y}_3 - \mathbf{Y}_O. \quad (14)$$

The normal vector, represented by the red line, is obtained via the cross product defined by $\mathbf{v}_3 = \mathbf{v}_1 \times \mathbf{v}_2$.

The drone's rotation matrix is formed as:

$$\mathbf{R}_{pose} = [\hat{\mathbf{v}}_1 \quad \hat{\mathbf{v}}_2 \quad \hat{\mathbf{v}}_3], \quad (15)$$

where $\hat{\mathbf{v}}_1, \hat{\mathbf{v}}_2$ and $\hat{\mathbf{v}}_3$ are the unit vectors of $\mathbf{v}_1, \mathbf{v}_2$ and \mathbf{v}_3 . The estimated rotation \mathbf{R}_{pose} and the centroid position $\mathbf{t}_{pose} = \mathbf{Y}_O$ are filtered using a Kalman filter to form the final 6DoF of the drone.

IV. DATASETS

All datasets summarized in Tab. I have been publicly released. Since acquiring real-world keypoint and 3D pose

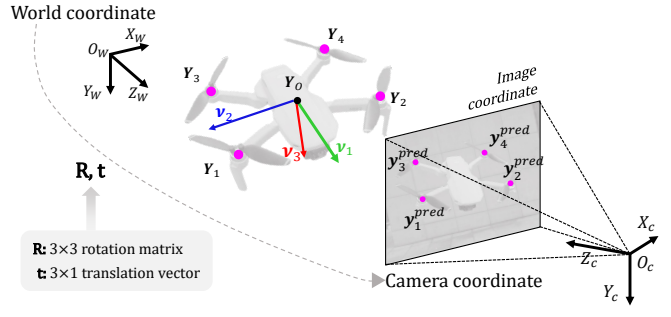


Fig. 6: Mapping 2D keypoints of the drone across image, camera, and world coordinate systems for 3D pose (6DoF) estimation.

ground truth for drones is challenging, we conducted experiments using a synthetic dataset with precise pose information. We provide two new drone datasets: 2Dronekey and 3DronePose. Further details of our datasets are provided in the supplementary material.

A. 2DroneKey (2D Images + keypoints)

2DroneKey is a dataset containing 2D drone images and propeller keypoints. We used a 3D program to generate a dataset 2DroneKey featuring Air2S and Mini2 drone models in five real-world backgrounds captured with a 360-degree camera. It consists of 10 sequences (Seq.1 to Seq.10), each with 1K frames, for a total of 10K frames. Rotation varies significantly, while translation remains nearly fixed. Images have a resolution of 1920×1080 .

B. 3DronePose (6DoF)

3DronePose provides three sequences (Seq. 11 to Seq. 13) that include 6DoF annotations for drones as well as keypoint annotations. Since no public 3D drone 6DoF dataset with keypoints has been available, we created a new dataset by adding 6DoF information to 2DroneKey, considering the drone sizes. This dataset includes various motion patterns and is designed to evaluate the performance of 3D pose estimation methods. Seq. 11 consists of linear motion without rotation, while Seq. 12 exhibits non-linear motion without rotation. In contrast, Seq. 13 involves non-linear motion with rotation. All images are captured at a resolution of 1920×1080 , ensuring high visual quality to enhance the accuracy of keypoint detection and 3D pose estimation.

V. EXPERIMENTAL RESULTS

A. Settings and Evaluation Metrics

All experiments were conducted on an Ubuntu system with an NVIDIA RTX 3060 GPU. Our model is based on a transformer encoder with 6 layers, 8 attention heads, and a

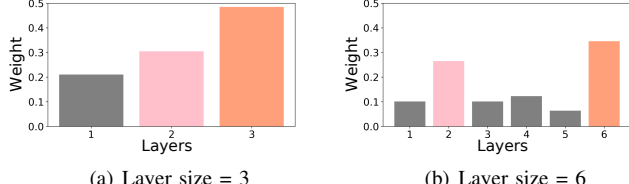
TABLE I: **Datasets.** The dataset is divided into 2DroneKey for keypoint detection and 3DronePose for pose estimation.

Sequences	2DroneKey		3DronePose		
	Sequences 1 to 5	Sequences 6 to 10	Sequence 11	Sequence 12	Sequence 13
Usage	keypoint detection train, valid and test		3D pose estimation validation		
Drone type	Air2S	Mini2	Mini2		
Frame	1,000 frames per sequence		500 frames	400 frames	300 frames
Translation	✓		✓	✓	✓
Rotation	✓		✓	✓	✓
Nonlinear translation			✓	✓	✓

TABLE II: Performance by number of layers.

Layer Size	SR_{90}^{kp}	SR_{95}^{kp}	AP^{kp}	Number of parameters
2	98.3	95.3	99.1	42.41M
3	99.1	96.5	99.4	59.21M
6	99.8	98.5	99.7	84.41M
8	99.7	97.8	99.6	101.22M
10	99.4	97.8	99.6	118.02M
12	98.2	94.9	99.14	134.82M

* Feature dimension: 1024; loss function: $\mathcal{L}_{pose}(\alpha = 5, D = 10)$



(a) Layer size = 3

(b) Layer size = 6

Fig. 7: **Gate weights analysis for different layer numbers.** ■ represents the highest weight values in intermediate layers (excluding the final layer), and ■ the final layer weights. This analysis highlights the significant contribution of both final and intermediate layers to keypoint learning, emphasizing the importance of features extracted at different network stages.

feature dimension of 1024. The model was trained for 100 epochs with a batch size of 8, a learning rate of 10^{-5} , and the Adam optimizer. For the pose-adaptive Mahalanobis loss function, we set $\alpha = 5$ and $D = 10$. These settings were determined as the optimal values through the ablation study.

In this study, object keypoint similarity (OKS) [7] is used to evaluate keypoint detection. OKS measures the similarity between predicted and ground truth (GT) keypoints on a scale from 0 to 1, where 1 indicates perfect alignment and 0 indicates no similarity. It is defined as:

$$OKS_{drone} = \frac{1}{K} \sum_{k=1}^K \exp \left(-\frac{d_k^2}{0.2\beta^2\gamma_k^2} \right) \quad (16)$$

where K is the number of keypoints and d_k is the Euclidean distance between predicted (\mathbf{y}^{pred}) and ground truth (\mathbf{y}^{GT}) keypoints. β represents the square root of the object area. Drones require more precise detection, so a stricter evaluation with a value of 0.2 is used. γ is the keypoint weight, we set to the same weight 1 for all drone propellers. To quantitatively evaluate keypoint detection, we used three metrics based on OKS:

- SR_{90}^{kp} : success rate at an OKS threshold of 0.90 (percentage of keypoints with $OKS \geq 0.90$).
- SR_{95}^{kp} : success rate at an OKS threshold of 0.95 (percentage of keypoints with $OKS \geq 0.95$).
- AP^{kp} : average precision (AP), computed as the mean OKS-based precision over multiple thresholds.

3D drone pose is represented in 6DoF, including rotation and translation. Rotation error is computed as the angle difference between the predicted and GT orientations. The mean angle error (MAE-angle) is averaged over all test sequences, where lower values indicate better accuracy. Translation error is measured as the Euclidean distance between predicted and GT positions. It is evaluated using root mean square error (RMSE) and mean absolute error (MAE-absolute), with lower values indicating higher accuracy.

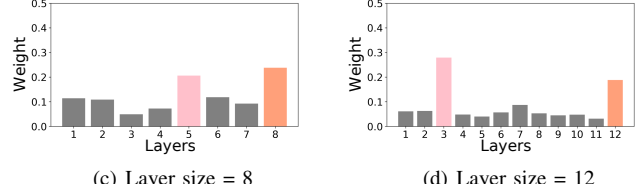
B. Ablation Studies of Keypoint Detection

1) **Encoder layers:** As shown in Tab. II, we ablated the number of encoder layers. In all evaluations, the embedding

TABLE III: Performance by embedding d .

Dimension	SR_{90}^{kp}	SR_{95}^{kp}	AP^{kp}	Number of parameters
128	98.1	93.6	99.1	27.92M
256	98.7	96.7	99.4	33.24M
512	97.3	95.5	99.1	46.63M
768	99.7	96.8	99.5	63.69M
1024	99.8	98.5	99.7	84.42M
2048	98.7	95.8	99.4	199.84M

* Number of layers: 6; loss function: $\mathcal{L}_{pose}(\alpha = 5, D = 10)$



(c) Layer size = 8

(d) Layer size = 12

TABLE IV: Performance comparison of loss functions. This table compares the performance of different loss functions for keypoint detection, including MSE loss, Gaussian loss, and pose-adaptive Mahalanobis loss.

Loss Type	Decay Type	SR_{90}^{kp}	SR_{95}^{kp}	AP^{kp}
MSE Loss	-	99.1	96.9	99.5
Gaussian Loss	Fixed	97.8	94	98.9
	Exp ($\alpha=5, D=10$)	99.4	97.4	99.5
Pose-adaptive Loss	Fixed	99.3	97.5	99.6
	Linear	97.1	95.4	98.9
	Exp ($\alpha=5, D=10$)	99.8	98.5	99.7
	Exp ($\alpha=10, D=10$)	92.1	88	95.3

* Number of layers: 6; feature dimension: 1024

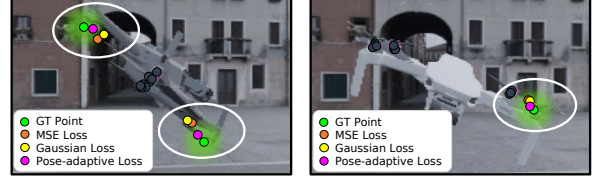


Fig. 8: **Visualization of keypoint detection with different loss functions.** Pose-adaptive Mahalanobis loss ● predicts keypoints closer to the GT ●, than MSE and Gaussian loss.

dimension was set to 1024, and the proposed loss function \mathcal{L}_{pose} was used. The results show that the 6-layer structure achieved the best performance while maintaining a well-balanced number of parameters. In contrast, models with 2 and 3-layer had fewer parameters but lower performance than the 6-layer. In the 8, 10, and 12-layer, performance decreased while the number of parameters increased. We extracted compact representations from each encoder layer and applied a gated sum to reflect layer importance. As shown in Fig. 7, the final layer (■) had the highest gate value, reflecting the integration of object-level information. However, the mid-layers (■) also showed high weights, especially in 6 and 8-layer models, where they were comparable to the final layer. Notably, in the 12-layer, mid-layer weights surpassed those of the final layer. This suggests that keypoint information is effectively learned in mid-layers, and gated summation plays a crucial role in balancing information across layers.

2) **Embedding dimension:** We conducted an ablation study on the embedding dimension. The encoder had 6-layer,

TABLE V: **Performance comparison of keypoint detection.** This table presents a comparative analysis of different methods for keypoint detection, categorized into object detectors, heatmap-based keypoint detectors, and coordinate-based keypoint detectors. (* 6 encoder layers + 6 decoder layers = 12 layers)

Approaches & Methods		Baseline	Layer	SR_{90}^{kp}	SR_{95}^{kp}	AP^{kp}
Object detector	YOLOv8 [22]	CNN	-	69.6	69.6	70.8
	DETR [23]	Transformer	12*	81.4	42.2	80.9
Heatmap-based keypoint detector	ViTPose [10]	Transformer	12	9.8	6.2	21.32
	TokenPose [12]	Transformer	12	32.5	31.4	43.6
Coordinate-based keypoint detector	SimCC [13]	CNN	-	37.3	34.3	59.1
	Ours	Transformer	6	99.8	98.5	99.68

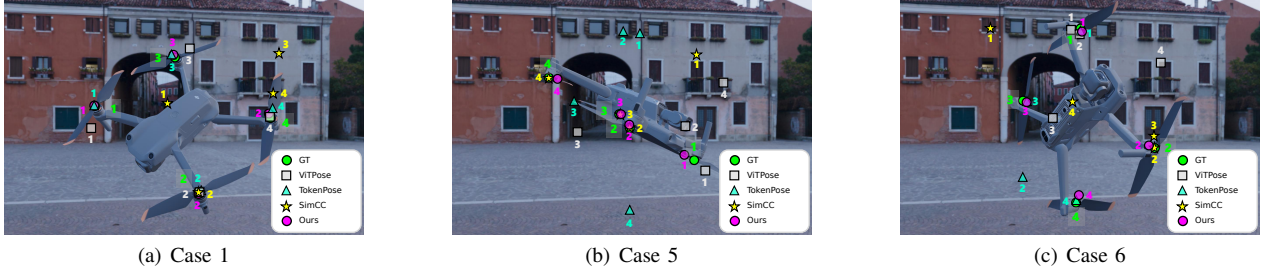


Fig. 9: **keypoint detection results for comparative experiments.** The predictions of ViTPose [10], TokenPose [12], SimCC [13] and the proposed method DroneKey (ours) are visualized alongside the GT in each case. The numbers (1 to 4) indicate the index of the keypoints. Further details of experimental results are provided in the supplementary material.

and the proposed \mathcal{L}_{pose} was used. Tab. III shows that the best performance is achieved at 1024 dimensions, with stable results at this size. Performance declines at 2048 dimensions, where the parameter count increases significantly. Lower dimensions (below 512) show reduced performance, making 1024 dimensions the optimal choice for balancing accuracy and computational efficiency.

3) **Loss function:** Tab. IV compares the impact of different loss functions on keypoint detection performance. The evaluated loss functions include MSE loss, Gaussian loss, and the proposed pose-adaptive Mahalanobis loss with various decay types: Fixed, Linear, Exp. For the exponential decay, we used the proposed scale function $S(t)$ as in Eq 9. Gaussian loss and pose-adaptive Mahalanobis loss incorporate decay factor (α) and scale factor (D) to improve prediction accuracy as training progresses. The proposed exponential decay enables flexibility in the early training stages for smoother convergence and becomes stricter later to enforce precise optimization and enhance final performance.

Gaussian loss does not estimate covariance Σ based on the keypoint distribution but instead uses an identity matrix. For Gaussian loss, the fixed setting resulted in lower performance than MSE loss, but applying exponential decay ($\alpha = 5, D = 10$) improved keypoint detection performances. The pose-adaptive loss with exponential decay ($\alpha = 5, D = 10$) achieved the best results, with AP^{kp} of 99.7%, SR_{90}^{kp} of 99.8%, and SR_{95}^{kp} of 98.5%. In contrast, increasing $\alpha = 10$ led to rapid decay in the early training stages, negatively affecting performance. Overall, the pose-adaptive Mahalanobis loss with exponential decay ($\alpha = 5, D = 10$) demonstrated robust performance even in extreme drone poses. It effectively addresses keypoint errors observed with MSE and Gaussian loss (Fig. 8). These findings confirm that dynamically adjusting the loss function during training enhances keypoint detection for complex poses.

C. Performance Comparison of Keypoint Detection

Tab. V compares keypoint detection methods: object detectors, heatmap-based, and coordinate-based approaches. The model was trained on 7K images, validated on 2K, and tested on 1K for consistency. Keypoint detection requires accurate detection (i.e., location (x, y) and size (w, h)) and correct ordering (i.e., keypoints labeled as 1, 2, 3, and 4). For drone propeller detection, we evaluated YOLOv8 [22] and DETR [23], assigning detector labels to encode the order. Both methods detected the location and size of the propellers but failed to predict their order due to the high visual similarity among them. DETR, leveraging global features, achieved an AP^{kp} of 80.9%, outperforming YOLOv8.

We also tested TokenPose [12] and ViTPose [10], which employ the heatmap regression approach. As depicted in Fig. 9, they struggled with accurate keypoint detection, either detecting incorrect locations (a-c) or confusing the order (c). Moreover, background clutter led to missed detections in both models. Transformers typically require large-scale training datasets of 300M+ images [24], and existing keypoint detection models are commonly trained on human COCO (56K+) [25]. Additionally, we set the OKS β value to 0.2 to account for the small keypoint regions of drone propellers. As a result, on the 2DroneKey (7K), TokenPose, ViTPose, and SimCC recorded low AP^{kp} due to the limited data and stricter evaluation criteria. The proposed DroneKey achieved AP^{kp} 99.68%, outperforming all previous methods. As shown in Fig. 9, it remains highly accurate, even in complex backgrounds and extreme poses. This experiment confirms that the proposed DroneKey efficiently learns to accurately detect drone keypoints even with a limited dataset.

D. Performance of 3D Pose Estimation

We estimated the 3D pose using a PnP solver based on keypoints. Due to low accuracy (see Tab. V), other methods were not considered for 3D pose reconstruction. Thus, we

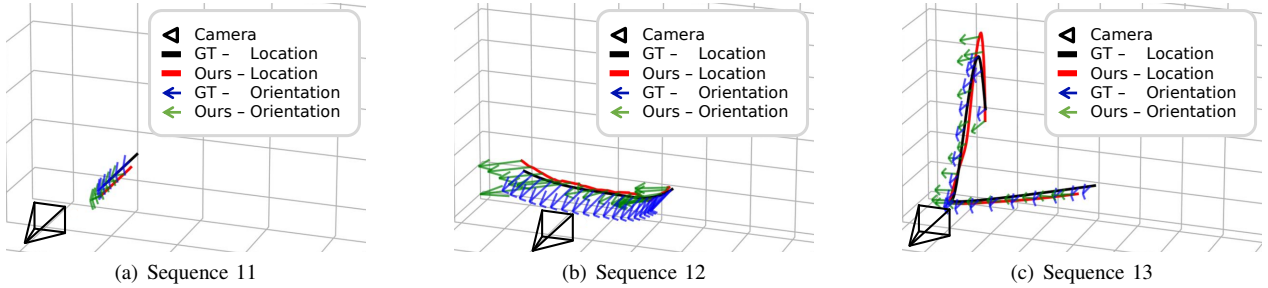


Fig. 10: Qualitative results of the drone 3D pose (6DoF) estimation based on the proposed method.

TABLE VI: Performance of 3D pose (6DoF).

6DoF	Metrics	Sequences (3DRONEPOSE)			Avg
		Seq. 11	Seq. 12	Seq. 13	
R_{pose}	MAE-angle ($^\circ$)	6.24	16.1	12.01	10.62
t_{pose}	RMSE (m)	0.228	0.212	0.346	0.221
	MAE-absolute (m)	0.08	0.073	0.11	0.076

conducted a 3D pose estimation experiment focusing on the proposed DroneKey. As summarized in Tab. VI, the results indicate an average R_{pose} MAE-angle error of 10.625° . For t_{pose} , the RMSE error was 0.221m, while the MAE-absolute error averaged 0.076m. Fig. 10 provides a qualitative comparison of the 3D drone pose estimation results.

In this experiment, rotation is visualized using only the drone camera's viewing axis for the clear comparisons. Additional quantitative results are provided in the supplementary materials. The results show that for all sequences, the estimated location and orientation closely match the ground truth. These findings confirm the effectiveness of our proposed method.

VI. CONCLUSIONS

This study proposes a drone-specific approach to address challenges in drone keypoint detection (Fig. 1 (a)). It enables 3D pose estimation using only geometric computations (e.g., PnP solver). A transformer is employed to learn spatial relationships and accurately distinguish propellers with similar visual. To enhance keypoint learning, we extract compact representations and apply gated sum in the keypoint head. Additionally, a pose-adaptive Mahalanobis loss function improves training performance across diverse drone poses. We released a synthetic drone keypoint dataset with real-world 360-degree backgrounds to address data shortages. Using only 6 encoder layers, the proposed model achieved real-time performance at 44 FPS with high accuracy (OKS AP^{kp} 99.68%, RMSE 0.221m, MAE-absolute 0.076m, MAE-angle 10.62°). The proposed DroneKey maintained high accuracy, demonstrating its suitability for real-time anti-drone systems.

Collecting real-world keypoint and 3D pose data is challenging, so we generated synthetic data with 360-degree images. Future study should focus on creating real-world datasets and handling drones with different propeller numbers. The proposed method estimates 3D pose using geometric calculations instead of a decoder. This emphasizes keypoint detection and enables robust pose estimation without extra training. However, keypoint errors can distort 3D pose estimation. To improve accuracy, we can consider adding a new 3D pose decoder in the future study. Since the proposed

methods run in real time, adding a decoder is expected to improve stability while maintaining performance.

ACKNOWLEDGMENT

This work was supported by the Institute of Information & Communications Technology Planning & Evaluation (IITP) grants funded by the Korea government (MSIT): the Artificial Intelligence Convergence Innovation Human Resources Development (IITP-2023-RS-2023-00256629) and the University ICT Research Center (ITRC) support program (IITP-2025-RS-2024-00437718). We appreciate the high-performance GPU computing support of HPC-AI Open Infrastructure via GIST SCENT.

REFERENCES

- [1] K. Wook et al. A study on the establishment of anti-drone concept and effective response system, Journal of the Korea Coast Guard, 2019.
- [2] ALBANIS, Georgios, et al. Dronepose: photorealistic uav-assistant dataset synthesis for 3d pose estimation via a smooth silhouette loss. ECCV, 2020, pp. 663-681.
- [3] JIN, Ren, et al. Drone detection and pose estimation using relational graph networks. Sensors, 2019, pp. 1479.
- [4] YIU, J, et al. UAV-Pose: A Dual Capture Network Algorithm for Low Altitude UAV Attitude Detection and Tracking. IEEE Access, 2023.
- [5] VASWANI, A. Attention is all you need. Advances in Neural Information Processing Systems, 2017.
- [6] BAN, Chung-Gi et al. Image classification using DETR based object-level feature. ICCAS, 2022, pp. 1297-1300.
- [7] XIAO, Bin; WU, Haiping; WEI, Yichen. Simple baselines for human pose estimation and tracking. In: Proceedings of the ECCV. 2018.
- [8] FU, Qiang et al. Robust pose estimation for multirotor UAVs using off-board monocular vision. IEEE Transactions on Industrial Electronics, 2017, pp. 7942-7951.
- [9] TOSHEV, Alexander et al. Deeppose: Human pose estimation via deep neural networks. CVPR, 2014, pp. 1653-1660.
- [10] XU, Yufei, et al. Vitpose: Simple vision transformer baselines for human pose estimation. Advances in Neural Information Processing Systems, 2022, pp. 38571-38584.
- [11] DOSOVITSKIY, Alexey. An image is worth 16x16 words: Transformers for image recognition at scale. ICLR, 2021.
- [12] LI, Yanjie, et al. Tokenpose: Learning keypoint tokens for human pose estimation. ICCV, 2021, pp. 11313-11322.
- [13] LI, Yanjie, et al. Simcc: A simple coordinate classification perspective for human pose estimation. ECCV, 2022, pp. 89-106.
- [14] TOMPSON, Jonathan J., et al. Joint training of a convolutional network and a graphical model for human pose estimation. Nips, 2014.
- [15] XU, Hailan, et al. Multi-Scale Coordinate Classification for Human Pose Estimation Based on Feature Reassembly. ACAIT, 2023.
- [16] HE, Kaiming, et al. Mask r-cnn. ICCV, 2017, pp. 2961-2969.
- [17] PAPAIANOANNDIS, Christos, et al. Fast CNN-based single-person 2D human pose estimation for autonomous systems. IEEE Transactions on Circuits and Systems for Video Technology, 2022, pp. 1262-1275.
- [18] SINGH, Anubhav, et al. Human pose estimation using convolutional neural networks. AICAI, IEEE, 2019, pp. 946-952.
- [19] XIE, Enze, et al. SegFormer: Simple and efficient design for semantic segmentation with transformers. Advances in neural information processing systems, 2021, pp. 12077-12090.
- [20] IM, Jinbae, et al. Egtr: Extracting graph from transformer for scene graph generation. CVPR, 2024, pp. 24229-24238.
- [21] LEPEITIT, Vincent; MORENO-NOGUER, Francesc; FUA, Pascal. EPnP: An accurate $O(n)$ solution to the PnP problem. International journal of computer vision, 2009, pp. 155-166.
- [22] G. Jocher, A. Chaurasia, and J. Qiu, Ultralytics YOLOv8, version 8.0.0, 2023. [Online]. Available: <https://github.com/ultralytics/ultralytics>. [Accessed: Feb. 16, 2025].
- [23] CARIÓN, Nicolas, et al. End-to-end object detection with transformers. ECCV, 2020, pp. 213-229.
- [24] TOUVRON, Hugo, et al. Training data-efficient image transformers distillation through attention. PMLR, 2021, pp. 10347-10357.
- [25] LIN, Tsung-Yi, et al. Microsoft COCO: Common Objects in Context. arXiv preprint arXiv:1405.0312, 2015.